Homogenization of Hydraulic Conductivity for Hierarchical Sedimentary Deposits at Multiple Scales

Transport in Porous Media

ISSN 0169-3913
Volume 87
Number 3

Transp Porous Med (2011)
87:717-737
DOI 10.1007/
s11242-010-9711-8

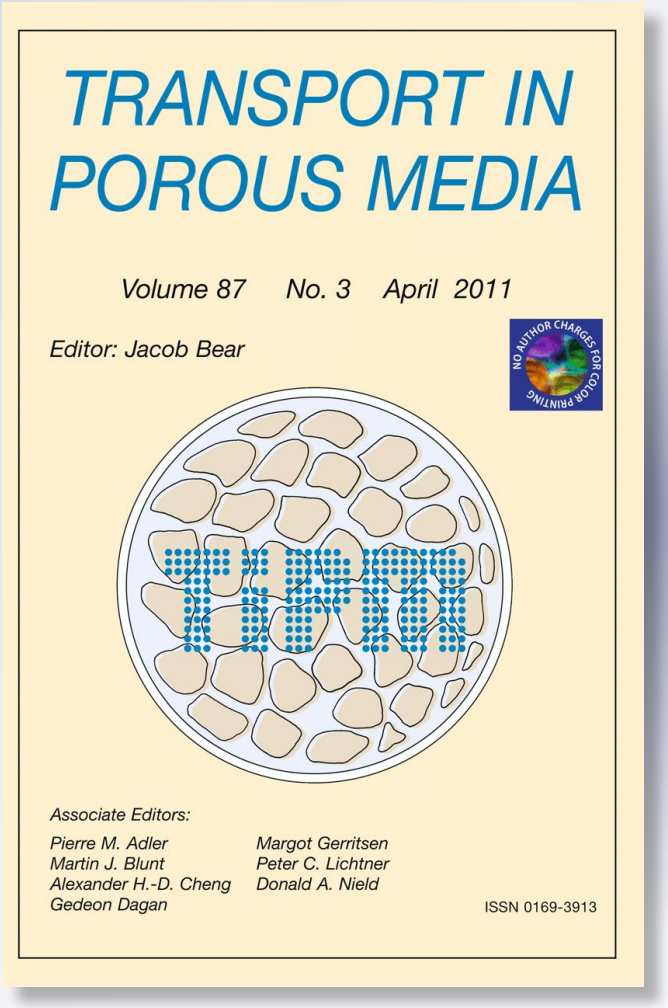

Springer

Transp Porous Med (2011) 87:717–737
DOI 10.1007/s11242-010-9711-8

Homogenization of Hydraulic Conductivity for Hierarchical Sedimentary Deposits at Multiple Scales

Ye Zhang · Baozhong Liu · Carl W. Gable

Received: 18 May 2010 / Accepted: 30 December 2010 / Published online: 14 January 2011

Abstract Based on a three-dimensional heterogeneous aquifer model exhibiting non-stationary, statistically anisotropic correlation, three hydrostratigraphic models (HSMs) are created within a sedimentary hierarchy. A geostatistical analysis of natural log conductivity ($\ln K$) is conducted for the units of the HSMs. Hydraulic conductivity is then upscaled using numerical and analytical methods. Increasing $\ln K$ variances are evaluated. Results suggest that for the aquifer model tested: (1) the numerical method is capable of upscaling irregular domains with reasonable accuracy for a $\ln K$ variance up to 7.0. (2) Accuracy of the upscaled equivalent conductivities ($\mathbf{K}^*$) and associated performance of the HSMs are sensitive to homogenization level, heterogeneity variance, and boundary condition. Variance is found to be the most significant factor impacting the accuracy of the HSMs. (3) Diagonal tensor appears a good approximation for the full-tensor $\mathbf{K}^*$. (4) For the HSM units, when the variance is low (less than 1.0), all analytical methods are nearly equally accurate; however, when variance becomes higher, analytical methods generally are less accurate.

Keywords Hydraulic conductivity · Heterogeneity · Upscaling · Equivalent conductivity · Sedimentary hierarchy

1 Introduction

Environmental and petroleum studies have documented that spatial variation in hydraulic conductivity (K), or conductivity heterogeneity, is the rule rather than exception in natural

Y. Zhang (✉)
University of Wyoming, 1000 University Ave., Laramie, WY 82071, USA
e-mail: yzhang9@uwyo.edu

B. Liu
University of Wyoming, Laramie, WY 82071, USA

C. W. Gable
Los Alamos National Lab, Los Alamos, NM 87545, USA

sedimentary rocks. In aquifers, conductivity heterogeneity is found to control the location and pathway of groundwater flow (thus the movement of dissolved solutes in groundwater). In petroleum reservoirs, heterogeneity of permeability is of interest. Since the advent of modern computers, subsurface fluid processes are evaluated quantitatively using simulation models. Such models are commonly constructed with site geological and/or geophysical data, populated with appropriate parameters (e.g., conductivity and storage coefficient in aquifers, permeability and rock/fluid compressibility in reservoirs), calibrated based on observed fluid potential and flow rate data, and then used for predictions for aquifer or reservoir management. However, detailed subsurface heterogeneity is rarely incorporated into the models, due to the prohibitive cost of conducting subsurface sampling over large spatial scales and computation limitation.

Because of the known impact of heterogeneity on subsurface fluid flow, some level of K (or permeability) variation is incorporated in models, though most do not account for heterogeneity down to the smallest resolvable continuum scale (e.g., core measurements). For example, heterogeneity is sometimes populated throughout a model grid via geostatistical means, i.e., each grid cell is given a grid conductivity which accounts for bulk flow behaviors arising out of the unresolved sub-grid heterogeneities. On the other hand, when multiple aquifer or reservoir layers exist, heterogeneity can be represented by a series of internally homogeneous units to represent important flow pathways or barriers. In petroleum studies, using outcrop, well log, or high-resolution seismic data, facies or facies assemblage modeling can identify zones of relative homogeneity at even finer scales. This second type of heterogeneity representation, relevant in field- and larger scale modeling, is referred to as a hydrostratigraphic model (HSM).

In sedimentary rocks, depositional structures can exist at multiple scales which determine the spatial variation of K. Division of HSM units is thus non-unique, their creation constrained by model scale, processes of interest (e.g., fluid flow versus species transport), computing power, or type and availability of site characterization data. Regardless of the simulation goal, equivalent conductivity (or equivalent permeability) is required for the model units, to represent the effect of unresolved, sub-unit-scale heterogeneity on bulk flow prediction. This upscaling should be distinguished from the body of work conducted in coarse-graining research (Sanchez-Vila et al. 1995, 1996; Wen and Gómez-Hernández 1996; Renard and de Marsily 1997; Durlofsky 2005; Sanchez-Vila et al. 2006). Typically, in such studies, a high-resolution geological model is upscaled to a coarsened flow simulation grid in order to achieve computation efficiency in flow modeling.

In this study, single-phase water flow is of interest, thus conductivity is the parameter evaluated. Based on a three-dimensional (3D) heterogeneous model exhibiting non-stationary, statistically anisotropic correlation structure, a set of nested HSMs is created within a sedimentary hierarchy. For units of these models, equivalent conductivity ($\mathbf{K}^*$) are estimated using numerical and analytical upscaling methods. A sensitivity analysis is conducted by scaling the heterogeneous model to multiple natural log conductivity ($\ln K$) variances. At each variance, upscaling is repeated. Both variance and homogenization level are thus evaluated to understand their impact on $\mathbf{K}^*$ and accuracy of the HSMs in single-phase predictions. Note that for two aquifer models, one with geometric connectivity and one without, an earlier study has compared their scaling characteristics using similar techniques (Zhang et al. 2010). The unique aspect of this study is the evaluation of sub-aquifer heterogeneities at multiple scales, which the earlier study did not address.

In the reminder of this article, creation of the models is described, followed by descriptions of a geostatistical analysis and the numerical and analytical upscaling methods. Section 3 presents the upscaled conductivities: those computed by the numerical method are verified

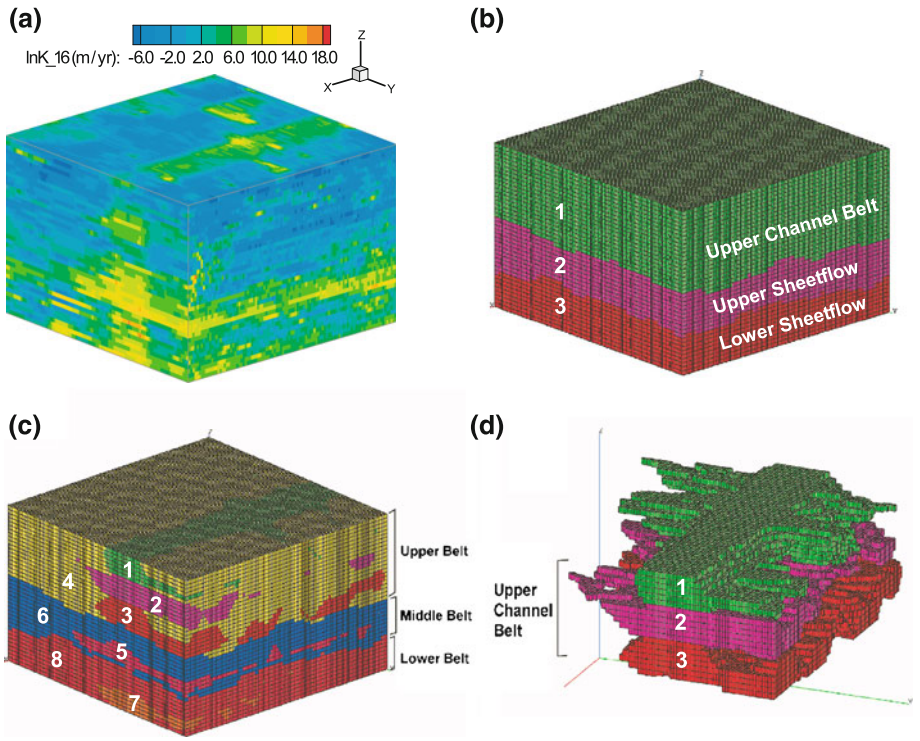

Fig. 1 **a** Heterogeneous model with local K in natural log scale (here, $\ln K$ variance = 16); **b** Depositional Model with 3 units: upper channel belt, upper sheetflow, and lower sheetflow. Unit ID is shown. **c** Facies Model with 8 units. Unit ID is shown. **d** Visualization of units 1, 2, and 3 of the Facies Model

by conducting flow simulations in all models. Accuracy of the HSMs in predicting flow rate and fluid potential of the heterogeneous model is discussed. Prediction sensitivity to $\ln K$ variance is highlighted. Linkage among conductivities homogenized at different scales is explored. Conductivity upscaled by analytical methods is presented next, their limitations discussed. Finally, results are summarized and directions for future research are presented.

2 Methods

2.1 Model Construction

Three HSMs are created from a heterogeneous model within a single grid structure: the heterogeneous model has spatially variable conductivities (Fig. 1a), the HSMs have homogenized units with upscaled $\mathbf{K}^*$ (Fig. 1b, c, d). Details on creating the heterogeneous model are described elsewhere (Zhang et al. 2010). Below sections describe the creation of the HSMs.

The HSMs are created within a 3-tier sedimentary hierarchy: (1) a *Full Aquifer Model* (1-unit model); (2) a *Depositional Model* (3-unit model) (Fig. 1b); and (3) a *Facies Model* (8-unit model) (Fig. 1c). Identification number for each unit is labeled on the models. In the facies and depositional models, all units are irregular, created with the following steps. First, we start with the most refined model—the Facies Model. Delineation of units in this

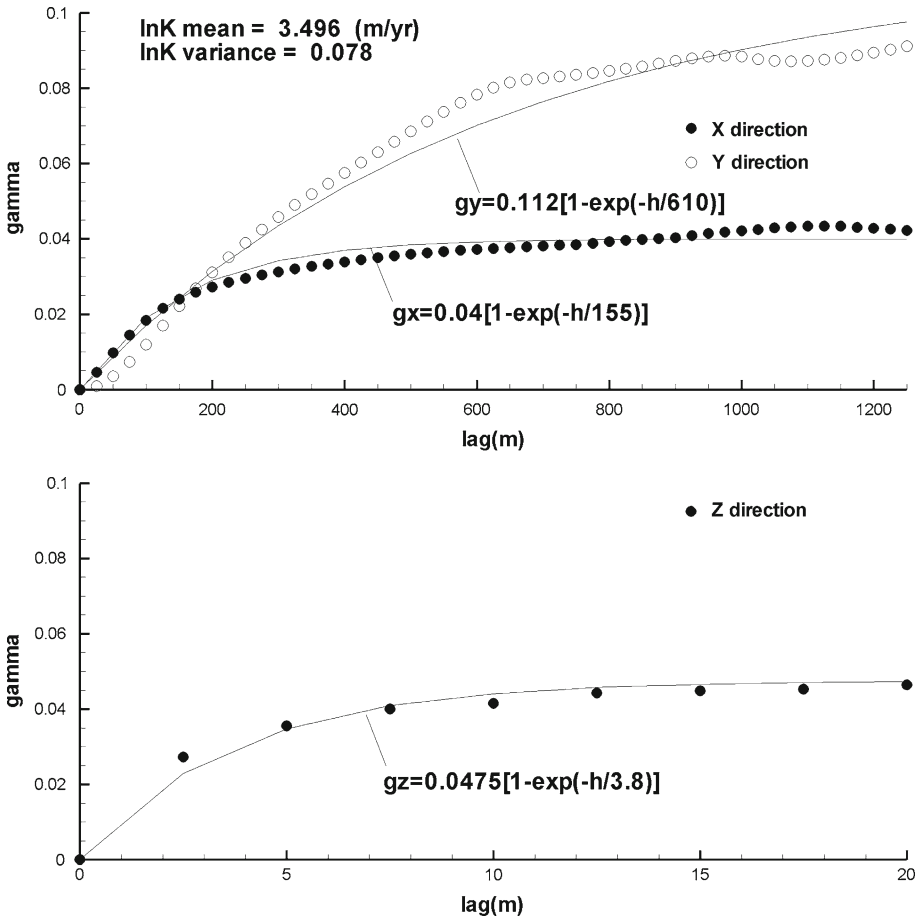

Fig. 2 Directional experimental variograms of $\ln K$ (*circles*) for the upper channel belt (unit 1 of the Depositional Model). Three exponential models are fitted (*curves*). Global aquifer $\ln K$ variance is 0.1. Since the upper channel belt is only a part of the aquifer, its variance is lower (0.078)

model is based on visual inspection of stratigraphic contacts and/or changes in dominant heterogeneity style. Four steps are used: (1) the heterogeneous model is dissected into 26 two-dimensional slices at $x = 10, 100, 200, \ldots, 2400, 2500$ m; (2) correlatable stratigraphic contacts are traced on each image, their coordinates (i.e., (y, z) values of points along the contacts) recorded at each x. For the 8 units of the Facies Model, 12 curvilinear contacts are defined on each image; (3) by pooling together all images, 12 correlated surfaces are created using Ordinary Kriging interpolation (for each surface, a global omnidirectional experimental variogram of z is computed and fitted with a Gaussian model whose parameters are used in kriging); (4) using the gridding toolbox *lagrit* (www.lagrit.lanl.gov), these surfaces are imported into the 3D grid and used to divide the model into different facies units.

Since the upper portion of the deposits appears more channelized than the lower portion, all cells of the Facies Model are recolored to assemble and regroup the units into 3 Depositional Model units: Upper Channel Belt, Upper Sheetflow Belt, and Lower Sheetflow Belt (Fig. 1b). Units 1, 2, 3 of the Facies Model become channel facies of unit 1 of the Depositional

Model, while unit 4 becomes the background floodplain facies of unit 1 of the same model. Unit 5 of the Facies Model is now sheetflow facies of unit 2 of the Depositional Model, while unit 6 is the background floodplain facies of the same unit. The Full Aquifer Model (not shown) incorporates all units of the Depositional Model. It has the highest level of hierarchy for which a natural analog could be a geological formation. Since only one unit exists in this model, it also has the greatest volume for conductivity homogenization.

In the above analysis, a set of sedimentary criteria is used to correlate and map the sub-aquifer hierarchy. The division adopted, however, is non-unique. For example, by creating more stratigraphic contacts within facies, a HSM can be created at sub-facies scale, and accordingly, units for homogenization will be more numerous. However, the current division reflects the current heterogeneity complexity in the aquifer. Since the mapping approach is flexible, as is the numerical upscaling method (presented next), the study methodology is applicable to any dataset and any interpretation.

In this study, the heterogeneous model is first scaled to 4 global $\ln K$ variances: 0.1, 1.0, 7.0, 16.0, spanning the full range of variability representing weakly to strongly heterogeneous deposits (Gelhar 1993). During this scaling, the same mean $\ln K$ value (3.67 m/y) is maintained. Thus, four populations of conductivity are created and subsequently upscaled. In a practical sense, this scaling reflects the certainty of heterogeneity pattern (e.g., from seismic interpretations), but uncertainty of the level of variability of heterogeneity (Milliken et al. 2007).

2.2 Spatial Correlations

Geostatistical characteristics of each unit of the HSMs are evaluated by computing three directional experimental $\ln K$ variograms: two horizontal (one along x, one along y), one vertical. Given the cellwise coloring of unit IDs, variogram computation for the units is straightforward, i.e., variogram pairs are selected not only based on separation vectors but also based on unit IDs (more details can be found in Zhang 2008). Variograms of the Full Aquifer model was presented in Zhang et al. (2010). Figure 2 presents the variograms of the Upper Channel Belt of the Depositional Model. In this figure, $\ln K$ variance is 0.1. Scaling of $\ln K$ variance will proportionally scale the variogram sill without affecting the correlation ranges. Similar variograms are computed for all the HSM units (not shown). With the exception of two lateral-direction periodic structures, all variograms exhibit exponential-like behavior, thus exponential models are fitted to the experimental variograms and directional integral scales are estimated (Table 1).

From the variograms, we observe: (1) both the integral scales and associated statistical anisotropy ratios (e.g., λ_x/λ_z, λ_y/λ_z) fall within the range found for natural fluvial deposits (Deutsch 2002), suggesting that the model grid cell size and aspect ratio are reasonable; (2) both horizontal integral scales are significantly larger than the vertical integral scale, $\ln K$ of all units is thus statistically anisotropic; (3) variogram spatial correlation is not axisymmetric, i.e., the two horizontal integral scales are not equal. For all units and at all scales, $\lambda_y > \lambda_x$[1]; (4) correlation characteristics of the HSM units are similar at different scales. With few exceptions, $\ln K$ variograms exhibit exponential rises towards the sills, which can be explained by the observed stratification (Fig. 1a). Detailed field mapping of conductivity

[1] A plausible explanation for the larger length of continuity along y is that sediment transport in the physical experiment from which the heterogeneous model of this study is derived occurred along the y-axis (Zhang et al. 2010). It is also possible that since the heterogeneous model is interpolated among 16 images perpendicular to y, y-directional continuity was enhanced by this procedure (Zhang et al. 2010).

Table 1 Statistical parameters of the 3 hydrostratigraphic models

Hydrostratigraphic models	Unit ID	Number of grid cells	Global ln$K$ variance[a]								Fitted integral scales (m)		
			0.1		1.0		7.0		16.0		λ_x	λ_y	λ_z
			E [ln$K$]	Var [ln$K$]	E [ln$K$]	Var [ln$K$]	E [ln$K$]	Var [ln$K$]	E [ln$K$]	Var [ln$K$]			
Full Aquifer Model	1	418241	3.668	0.1	3.668	1.0	3.668	7.0	3.668	16.0	155.0	690.0	5.0
Depositional Model	1	204728	3.496	0.078	3.124	0.784	2.229	5.487	1.492	12.543	155.0	610.0	3.8
	2	99669	3.861	0.066	4.280	0.662	5.288	4.632	6.117	10.586	140.0	900.0	12.0
	3	113844	3.807	0.063	4.110	0.629	4.837	4.404	5.436	10.066	200.0	900.0	12.0
Facies Model	1	16696	3.724	0.046	3.846	0.458	4.140	3.208	4.382	7.333	155.0	610.0	3.5
	2	22559	3.757	0.048	3.949	0.482	4.412	3.373	4.793	7.709	135.0	320.0	3.0
	3	28221	3.771	0.037	3.995	0.373	4.534	2.612	4.977	5.971	135.0	700.0	3.4
	4	137252	3.368	0.046	2.721	0.464	1.163	3.248	0.119	7.423	155.0	250.0	3.0
	5	17422	4.168	0.027	5.250	0.266	7.853	1.859	9.995	4.248	155.0	275.0	7.5
	6	82247	3.796	0.050	4.075	0.504	4.744	3.529	5.295	8.067	155.0	720.0	15.0
	7	13070	4.079	0.044	4.967	0.437	7.106	3.056	8.865	6.984	230.0	300.0	3.0
	8	100774	3.772	0.055	3.998	0.546	4.543	3.825	4.991	8.743	330.0	350.0	16.0

[a]Hydraulic conductivity (K) is in m/y. Global ln$K$ variance is the variance of ln$K$ for the full aquifer model. E [ln$K$] is the mean ln$K$. Var [ln$K$] is the variance of ln$K$

in channelized systems has linked such behaviors to multiple scales of juxtaposing units of contrasting conductivities (Ritzi and Allen-King 1986).

Correlation parameters for each unit, along with the mean and variance of $\ln K$, will be used by select analytical methods to predict an equivalent or effective conductivity, to be compared to the results of numerical upscaling. Though not presented, histograms of $\ln K$ of most units are unimodal, with probability densities approaching normal distributions. Thus, though the conductivity field as a whole exhibits non-multiGaussian characteristics (e.g., distinct existence of channel connectivity, heterogeneity non-stationarity ranging from channel to sheetflow dominated), its univariate and bivariate statistics closely satisfy most analytical theory requirements (Sect. 2.4). This is because bivariate correlation functions cannot distinguish either the existence, or lack of existence, of important spatial connectivity as observed in natural heterogeneity (Knudby and Carrera 2005, 2006).

2.3 Numerical Upscaling

To calculate an equivalent conductivity ($\mathbf{K}^*$), numerical upscaling is conducted by simulating flow in the heterogeneous model, based on and in extension to earlier studies (Zhang et al. 2006, 2010). To find $\mathbf{K}^*$ for a HSM unit, a series of single-phase, steady-state, and incompressible flow simulations are conducted in the heterogeneous model by varying the boundary condition along the model periphery. An equivalent $\mathbf{K}^*$ is obtained by incorporating results from all simulations. For each unit, a set of equations is assembled, consisting of spatially averaged directional hydraulic gradients, Darcy fluxes, and equivalent conductivity tensor components:

$$
\begin{bmatrix}
\langle \partial h/\partial x\rangle_1 & \langle \partial h/\partial y\rangle_1 & \langle \partial h/\partial z\rangle_1 & 0 & 0 & 0 & 0 & 0 & 0 \\
0 & 0 & 0 & \langle \partial h/\partial x\rangle_1 & \langle \partial h/\partial y\rangle_1 & \langle \partial h/\partial z\rangle_1 & 0 & 0 & 0 \\
0 & 0 & 0 & 0 & 0 & 0 & \langle \partial h/\partial x\rangle_1 & \langle \partial h/\partial y\rangle_1 & \langle \partial h/\partial z\rangle_1 \\
\langle \partial h/\partial x\rangle_2 & \langle \partial h/\partial y\rangle_2 & \langle \partial h/\partial z\rangle_2 & 0 & 0 & 0 & 0 & 0 & 0 \\
0 & 0 & 0 & \langle \partial h/\partial x\rangle_2 & \langle \partial h/\partial y\rangle_2 & \langle \partial h/\partial z\rangle_2 & 0 & 0 & 0 \\
0 & 0 & 0 & 0 & 0 & 0 & \langle \partial h/\partial x\rangle_2 & \langle \partial h/\partial y\rangle_2 & \langle \partial h/\partial z\rangle_2 \\
\cdots & \cdots & \cdots & \cdots & \cdots & \cdots & \cdots & \cdots & \cdots \\
\langle \partial h/\partial x\rangle_m & \langle \partial h/\partial y\rangle_m & \langle \partial h/\partial z\rangle_m & 0 & 0 & 0 & 0 & 0 & 0 \\
0 & 0 & 0 & \langle \partial h/\partial x\rangle_m & \langle \partial h/\partial y\rangle_m & \langle \partial h/\partial z\rangle_m & 0 & 0 & 0 \\
0 & 0 & 0 & 0 & 0 & 0 & \langle \partial h/\partial x\rangle_m & \langle \partial h/\partial y\rangle_m & \langle \partial h/\partial z\rangle_m \\
0 & 1 & 0 & -1 & 0 & 0 & 0 & 0 & 0 \\
0 & 0 & 1 & 0 & 0 & 0 & -1 & 0 & 0 \\
0 & 1 & 0 & 0 & 0 & 1 & 0 & -1 & 0
\end{bmatrix}
\cdot
\begin{Bmatrix}
K_{xx} \\ K_{xy} \\ K_{xz} \\ K_{yx} \\ K_{yy} \\ K_{yz} \\ K_{zx} \\ K_{zy} \\ K_{zz}
\end{Bmatrix}
= -
\begin{Bmatrix}
\langle q_x\rangle_1 \\ \langle q_y\rangle_1 \\ \langle q_z\rangle_1 \\ \langle q_x\rangle_2 \\ \langle q_y\rangle_2 \\ \langle q_z\rangle_2 \\ \cdots \\ \langle q_x\rangle_m \\ \langle q_y\rangle_m \\ \langle q_z\rangle_m \\ 0 \\ 0 \\ 0
\end{Bmatrix}
\tag{1}
$$

where $\langle\,\rangle$ represents spatial averaging among grid cells of a HSM unit; q_x, q_y, q_z are components of the Darcy flux; h is hydraulic head; subscripts $1, 2, \ldots, m$ denote flow experiments

driven by different global boundary conditions; $K_{xx}, \ldots, K_{zz}$ are components of the equivalent $\mathbf{K}^*$. To obtain a unique solution, the total number of flow experiments m must be ≥ 3. For the above non-square system (e.g., $\mathbf{Ax} = \mathbf{b}$), Eq. 1 is solved via least square solution, i.e., $\mathbf{x}$ is determined by minimizing the 2-norm of the residual vector $\mathbf{r} = \mathbf{Ax} - \mathbf{b}$, where 2-norm is defined as $||\mathbf{r}||_2 = \sqrt{\sum_{i=1}^{3m+3}(r_i^2)}$.

Within the context of the upscaling literature, the above method is global in nature: $\mathbf{K}^*$ of a particular upscaling domain (e.g., a HSM unit) is calculated using averages of head gradients and fluxes which are computed from global flow simulations that extend beyond the particular domain. Further, symmetry in $\mathbf{K}^*$ is ensured by adding 3 constraint equations on the off-diagonal terms. This procedure is a more natural approach compared to those of our earlier studies (symmetry is imposed after solving the off-diagonal components), although scaling of the constraint equations by a number consistent with the magnitude of the gradient components may be necessary to reduce numerical truncation error. As discussed by Wen et al. (2003), positive-definiteness of $\mathbf{K}^*$ cannot be assured by this procedure. Thus, for each HSM unit, after $\mathbf{K}^*$ is computed by Eq. 1, test is conducted to ensure that the result is physically correct (e.g., eigen values of $\mathbf{K}^*$ are positive).

The size of Eq. 1 is controlled by m which is ideally a large number simulating many boundary conditions. The system is thus subjected to many types of flow stimulation so that a representative conductivity may be found that is less dependent on the boundary condition. In earlier studies, we found that when the upscaling domain was large compared to $\ln K$ integral scales, $\mathbf{K}^*$ became insensitive to boundary condition and the number of flow experiments, thus smaller m may be used (Zhang et al. 2006). However, the set of experiments must be carefully chosen so that each will result in a flow field that is distinct from the others. This means that similar boundary condition will not be used, e.g., imposing a higher gradient to drive flow compared to a previous experiment using a lower gradient. Moreover, although the global method is computationally more expensive than the various local methods, they can be more accurate since flow channeling due to conductivity connection outside the upscaling domain can be accounted for in computing $\mathbf{K}^*$. This is affirmed by observations that accuracy of a local method improves when the size of the upscaling region surrounding each grid cell increases (Wen et al. 2003).

Numerical upscaling results are compared to the results of several analytical methods developed under mean uniform flow conditions, thus linear flood patterns are used in the flow experiments (analytical expressions developed for radial flows with source or sink terms are not investigated). For each HSM unit, Eq. 1 is assembled based on 3 sets of global boundary conditions ($m = 3$): (1) x-flow (specified heads along the left and right faces of the model; no-flow on all other faces); (2) y-flow (specified heads along the front and back faces; no-flow on all other faces); (3) z-flow (specified heads along the top and bottom faces; no-flow on all other faces). More details on these experiments and the effort involved in code verification can be found in Zhang et al. (2010).

2.4 Analytical Upscaling

Several analytical methods exist that are applicable to upscaling statistically anisotropic media. For example, power law was proposed as an approach for equivalent conductivity estimation (Journel et al. 1986):

$$K_{jj} = \left[\frac{1}{N}\sum_{i=1}^{N} K_i^{p_j}\right]^{1/p_j} \quad (j = 1, \ldots, 3) \tag{2}$$

where N is number of local conductivities (K_i), K_{jj} is principal components of the equivalent conductivity, p_j is the corresponding directional power-averaging exponent. $-1 \le p_j \le 1$: when $p_j = -1$, K_{jj} is the harmonic mean (K_H); when $p_j = 1$, K_{jj} is the arithmetic mean (K_A); when $p_j \to 0$ in the limit, K_{jj} becomes the geometric mean (K_G). For statistically anisotropic media, p_j is estimated by Ababou (1991) as:

$$p_j = 1 - \frac{2}{3}\frac{\lambda_\mathrm{Harmo}}{\lambda_j} \quad (j = 1, \ldots, 3) \tag{3}$$

where λ_j is directional $\ln K$ integral scales, λ_Harmo is their harmonic mean estimated by:

$$\lambda_\mathrm{Harmo} = \left[\frac{1}{3}\sum_{j=1}^{3}\lambda_j^{-1}\right]^{-1} \tag{4}$$

Equations 2–4 can be used to predict equivalent conductivity principal components, given the local conductivities and directional $\ln K$ integral scales.

For multiGaussian media, Desbarats (1992) also proposed a power law method, although the power-averaging exponents were obtained from numerical upscaling:

$$\ln(K_{jj}) = \mu_f + \frac{p_j}{2}\sigma_f^2 \qquad (j = 1, \ldots, 3) \tag{5}$$

where μ_f and σ_f^2 are expected value and variance of local point-scale $\ln K$, respectively. In this study, Eq. 5 is tested by applying the directional exponent (p_j) obtained from Eq. 2—p_j is calculated by equating Eq. 2 with the principal components of the upscaled $\mathbf{K}^*$.

Based on the Green's function, another expression using p_j was derived for a multiGaussian medium of a large extent (i.e., domain length greater than $\ln K$ integral scales) (Noetinger and Haas 1996):

$$K_{jj} = K_\mathrm{G}\exp(p_j\sigma_f^2/2) \quad (j = 1, \ldots, 3) \tag{6}$$

Equation 6 was numerically verified to be accurate for $\ln K$ variances up to 1.0.

In a stationary medium with low variance, an effective conductivity expression was developed based on K_G, σ_f^2, and $\ln K$ integral scales (Gelhar and Axness 1983):

$$K_{jj} = K_\mathrm{G}\left[1 + \sigma_f^2\left(\frac{1}{2} - g_{jj}\right)\right] \quad (j = 1, \ldots, 3) \tag{7}$$

where g_{jj} is a complex multidimensional integral. For an axisymmetrical medium (e.g., $\lambda_1 = \lambda_2 > \lambda_3$) with exponential correlation functions, g_{jj} becomes:

$$\begin{aligned} g_{11} = g_{22} &= \frac{1}{2}\frac{1}{\rho^2 - 1}\left[\frac{\rho^2}{\sqrt{\rho^2 - 1}}\tan^{-1}(\sqrt{\rho^2 - 1}) - 1\right] \\ g_{33} &= \frac{\rho^2}{\rho^2 - 1}\left[1 - \frac{1}{\sqrt{\rho^2 - 1}}\tan^{-1}(\sqrt{\rho^2 - 1})\right] \end{aligned} \tag{8}$$

where $\rho = \lambda_1/\lambda_3 > 1$. This result was tested and expanded by prior authors, e.g., see review in Zhang (2002). For statistically anisotropic media, it was found accurate for low variances (e.g., less than 1.0). In this study, λ_x and λ_y are averaged to obtain a λ_1, representing a horizontal integral scale from modeling an omnidirectional horizontal variogram. Further, based on the Landau–Lifshitz conjecture, a high variance version of Eq. 7 is postulated, which treats the two terms within the brackets of Eq. 7 as part of a series expansion of an exponential

function: $K_{jj} = K_G \exp\left[\sigma_f^2 \left(\frac{1}{2} - g_{jj}\right)\right]$ (Gelhar and Axness 1983). This formulation has not been tested extensively.

Following the same arguments of Gelhar and Axness (1983), a simplified formula is proposed and generalized to higher variances (Ababou 1996):

$$K_{jj} = K_G \exp\left[\sigma_f^2 \left(\frac{1}{2} - \frac{1}{3}\frac{\lambda_{\text{Harmo}}}{\lambda_j}\right)\right] \quad (j = 1, \ldots, 3) \tag{9}$$

Among the formulations, those based on stochastic theories aim to predict an ensemble effective conductivity of a random field, thus rigorous comparison between equivalent and effective conductivity will require a stochastic Monte Carlo analysis. In this study, rather than validating theories, we are interested in whether theories can be used to predict properties consistent with upscaling results from a single realization, following Zhang et al. (2006), Desbarats and Srivastava (1991). Within the stochastic framework, an argument can also be made that in evaluating single realizations, if the domain size is large compared to $\ln K$ integral scale (this has been assured by the geostatistical analysis; Table 1), an ergodic limit can be reached whereby deterministic spatial average coincides with ensemble average.

3 Results and Discussions

3.1 Upscaled Conductivities

For each unit of the HSMs, $\mathbf{K}^*$ is computed with Eq. 1, at 4 global $\ln K$ variances ($\sigma_f^2 = 0.1, 1.0, 7.0, 16.0$). Since conductivity must be positive definite, Cholesky factorization is used to test $\mathbf{K}^*$. With four exceptions, the majority of $\mathbf{K}^*$ (44 tensors) passes the test (Table 2 lists the principal components). The four that fail the test belong to unit 3 of the Depositional model and units 5, 7, and 8 of the Facies model, respectively, when $\sigma_f^2 = 16.0$. A common characteristics among them is an extremely small and negative K_{33} (principal component of $\mathbf{K}^*$ along z), compared to a positive and much larger K_{11} (principal component along x) and K_{22} (along y). Since 16 is considered a high variance, a likely cause for non-positive-definiteness is extreme flow channeling in the horizontal direction. In the aquifer model, a prior percolation analysis has identified a high-K connected structure spanning the lower domain along x—in the same region of the model containing these units (Zhang et al. 2010). At the same high variance, however, eight other units pass the test—these are located outside the spanning cluster. It is likely that the upscaled $\mathbf{K}^*$ is inaccurate when high variance coincides with geometric connectivity. These four tensors are excluded in the following analysis.

For all units, at all variances, most $\mathbf{K}^*$ are diagonally dominant reflecting horizontal stratification (Fig. 1a). Since diagonal dominance of upscaled $\mathbf{K}^*$ is an indication that $\ln K$ statistical axes are aligned with the global coordinate axes (Gelhar 1993), geostatistical analysis of this study is thus appropriate (it is carried out independently of the upscaling calculations). Since most analytical methods are based on the same assumption, diagonal dominance simplifies the comparison between numerical and analytical results.

$\mathbf{K}^*$ computed for the Full Aquifer Model are compared to the diagonal tensors computed for the same model using the Simple Laplacian (SL) method (Renard and de Marsily 1997). SL is a local method that is applicable to upscaling rectangular or box-shaped media. It is used to compute K_{xx}, K_{yy}, and K_{zz} of the Full Aquifer Model. Note that when applying Eq. 1 to the full aquifer, the global method is reduced to a local method. Due to diagonal dominance, K_{xx}, K_{yy}, and K_{zz} are comparable with K_{11}, K_{22}, and K_{33}. For the Full Aquifer

Table 2 Equivalent conductivity principal components computed with Eq. 1 for all the HSM units

Stratigraphic Models	Unit ID	Deposition type	Global ln$K$ variance											
			0.1			1.0			7.0			16.0		
			K_{11}[a]	K_{22}	K_{33}	K_{11}	K_{22}	K_{33}	K_{11}	K_{22}	K_{33}	K_{11}	K_{22}	K_{33}
Aquifer	Eq. 1	A fluvial system	40.968	40.101	38.153	60.736	50.320	33.434	514.172	185.345	34.052	5201.000	706.500	88.800
Model	SL[b]		40.981	40.147	38.434	60.747	50.432	34.295	512.724	185.896	36.176	5183.03	713.983	96.440
Depositional Model	1	Channelized	34.130	33.318	42.781	32.556	26.047	46.955	93.408	25.750	65.341	388.854	27.024	179.395
	2	Sheetflow	48.970	47.155	35.105	96.543	76.127	22.766	1132.100	345.000	5.100	13903.000	1413.00	4.000
	3	Sheetflow	46.266	46.072	32.477	80.155	70.930	18.280	732.574	326.337	2.579	**6249.800**	**1142.600**	**−0.500**
Facies Model	1	Channel	42.100	29.823	36.670	55.661	18.811	24.567	202.011	15.190	7.528	898.478	10.120	18.068
	2	Channel	43.657	33.910	43.457	63.875	26.218	47.883	320.484	22.310	67.934	1349.500	23.500	283.800
	3	Channel	44.035	34.844	46.651	62.674	28.861	61.921	245.360	28.183	97.345	1159.400	37.400	174.400
	4	Floodplain	29.591	33.336	42.623	18.656	26.333	46.513	12.980	27.221	65.867	7.858	34.948	186.592
	5	Sheetflow	65.344	51.742	33.610	212.079	96.264	19.762	4744.400	457.400	2.800	**71313.000**	**1714.000**	**−1.000**
	6	Background[c]	45.547	46.184	35.422	72.991	71.816	23.403	434.329	320.068	5.545	2977.700	1337.700	4.200
	7	Sheetflow	59.965	47.961	32.323	171.447	80.877	17.988	3387.100	460.900	2.400	**34754.000**	**1858.000**	**−1.000**
	8	Background[c]	44.485	45.847	32.497	68.334	69.900	18.318	401.014	315.427	2.595	**2691.200**	**1090.200**	**−0.700**

For the Full Aquifer Model, the principal components are also computed with the Simple Laplacian Method. Four of the conductivity tensors, tested to be non-positive-definite, are emphazised in *bold*

[a] All conductivity principal components are in units of m/yr; K_{11}, K_{22}, and K_{33} are aligned approximately with the global x, y, and z axes, respectively

[b] Simple Laplacian Method of Wen and Gómez-Hernández (1996) which computes a diagonal tensor for rectangular or box shaped media

[c] Background facies with lower conductivity can be distinguished from the high-K sheetflow deposit

model, at all variance levels, principal components of $\mathbf{K}^*$ are very close to those computed by the SL method. This serves to verify Eq. 1 for this model.

Comparing the principal components of $\mathbf{K}^*$ of the Full Aquifer Model with those of the Depositional and Facies models, their magnitudes are consistent across scales. Based on the volumes of the units (i.e., number of grid cells within), weighted arithmetic averages of appropriate sub-hierarchy conductivity components are calculated (Table 3). These weighted averages are compared to the corresponding upscaled conductivities of the encompassing unit(s) of higher hierarchy. A set of percent relative errors (RE) is calculated. For example, at the same variance, K_{11} of the Full Aquifer Model is compared to a weighted average of K_{11} of the 3 units of the Depositional Model and a weighted average of K_{11} of the 8 units of the Facies Model, respectively; K_{11} of unit 1 of the Depositional Model is compared to a weighted average of K_{11} of units 1, 2, 3, 4 of the Facies Model, etc.

Results suggest that for the given variance range (0.1–7.0), RE is extremely small (often less than 0.1%), thus equivalent conductivity principal components of the HSM units at different scales are related by volume-weighted arithmetic means. To our knowledge, this is the first time such a relationship is revealed among conductivities of irregular deposits. It is of interest to note that though harmonic averaging is a popular estimator to relate vertical conductivity at different scales, it is found inaccurate here, particularly when the system variance is high (both weighted harmonic mean and harmonic mean have been tested for which RE reaches 86% when $\sigma_f^2 = 7.0$). However, whether this observation is generalizable to other heterogeneities requires additional studies. Since $\mathbf{K}^*$ of the Full Aquifer model is verified by the SL method, this multiscale comparison serves to partially verify $\mathbf{K}^*$ computed for the facies and depositional models.

Finally, as part of the upscaling procedure, flow simulations are conducted in the heterogeneous model at increasing variances. When $\sigma_f^2 > 1.0$, preferential flow is observed in the lower portion of the model. In this region (i.e., units 2 and 3 of the Depositional Model and units 5–8 of the Facies Model), K_{33} consistently decreases with variance while K_{11} and K_{22} consistently increases with variance. This results in an increasingly larger lateral:vertical anisotropy ratio with variance (Fig. 3). A prior percolation analysis identified these deposits as not only laterally extensive, but also domain-spanning. As variance increases, fluid flow becomes increasingly channeled into the connected high-K cells, resulting in increasingly significant lateral flow while vertical flow is subdued. Preferential flow is thus characterized by increasing anisotropy ratios of $\mathbf{K}^*$, which exists in the domain-spanning deposits.

3.2 Flow Verification Tests

To assess the accuracy of the upscaled $\mathbf{K}^*$ and associated HSMs to predict flow responses of the heterogeneous model, single-phase (water), steady-state, and incompressible flow simulations are conducted in all models, for variances up to 7.0. Boundary conditions used are the same as those chosen for the upscaling analysis. In the HSMs, full tensor $\mathbf{K}^*$ is assigned to each unit. The tests are conducted with Eclipse 300 (2009 Version) (Schlumberger 2009), a general-purpose simulator. To create steady-state flow, the Fetkovich Aquifer Facility is used to set up a Constant-Head Darcy test, by driving flow from two opposing sides of the model (each side is connected to an external aquifer of a fixed fluid potential,[2]) while all other sides are no-flow boundaries.

[2] Fluid potential (Φ) is related to the hydraulic head ($\Phi = \rho g h$). For a chosen set of reservoir depth and datum, same fluid potentials are fixed at the external aquifers for all models. A potential gradient is then established in the model which drives flow.

Table 3 Equivalent conductivity of the Full Aquifer Model and units of the Depositional Model, created from volume-weighted arithmetic averaging of sub-unit conductivity computed with Eq. 1

	Global ln$K$ variance								
	0.1			1			7		
	K_{11}	K_{22}	K_{33}	K_{11}	K_{22}	K_{33}	K_{11}	K_{22}	K_{33}
Full Aquifer Model	weighted by Deposition $\mathbf{K}^*$ (3 units)								
Weighed Arith. Mean[a]	40.970	40.087	38.147	60.761	50.198	33.385	514.913	183.648	33.902
Relative Error (%)[b]	0.004	0.035	0.016	0.041	0.242	0.145	0.144	0.916	0.442
Full Aquifer Model	weighted by Facies $\mathbf{K}^*$ (8 units)								
Weighed Arith. Mean	40.989	40.093	38.149	61.029	50.256	33.407	531.676	185.043	34.056
Relative Error (%)	0.050	0.019	0.011	0.482	0.127	0.082	**3.404**	0.163	0.011
Unit 1 of Depo. Model	weighted by Facies $\mathbf{K}^*$ (units 1, 2, 3, 4)								
Weighed Arith. Mean	34.152	33.321	42.785	32.724	26.055	46.998	94.313	25.831	65.676
Relative Error (%)	0.065	0.008	0.009	0.517	0.032	0.092	0.968	0.316	0.513
Unit 2 of Depo. Model	weighted by Facies $\mathbf{K}^*$ (units 5, 6)								
Weighed Arith. Mean	49.007	47.156	35.105	97.303	76.089	22.767	1187.723	344.073	5.065
Relative Error (%)	0.077	0.001	0.001	0.788	0.049	0.002	**4.913**	0.269	0.683
Unit 3 of Depo. Model	weighted by Facies $\mathbf{K}^*$ (units 7, 8)								
Weighed Arith. Mean	46.262	46.090	32.477	80.172	71.160	18.280	743.835	332.128	2.573
Relative Error (%)	0.008	0.038	0.000	0.021	0.325	0.001	**1.537**	**1.775**	0.248

RE greater than 1% are highlighted with bold letter

[a] Weighted Arithmetic Means of sub-unit conductivity components were based on volume which was represented by the number of grid cells mapped for the units (Table 1)

[b] Relative Error (%) is defined as: $|K_{\text{weighted}} - K_{\text{upscaled}}|/K_{\text{upscaled}} * 100\%$

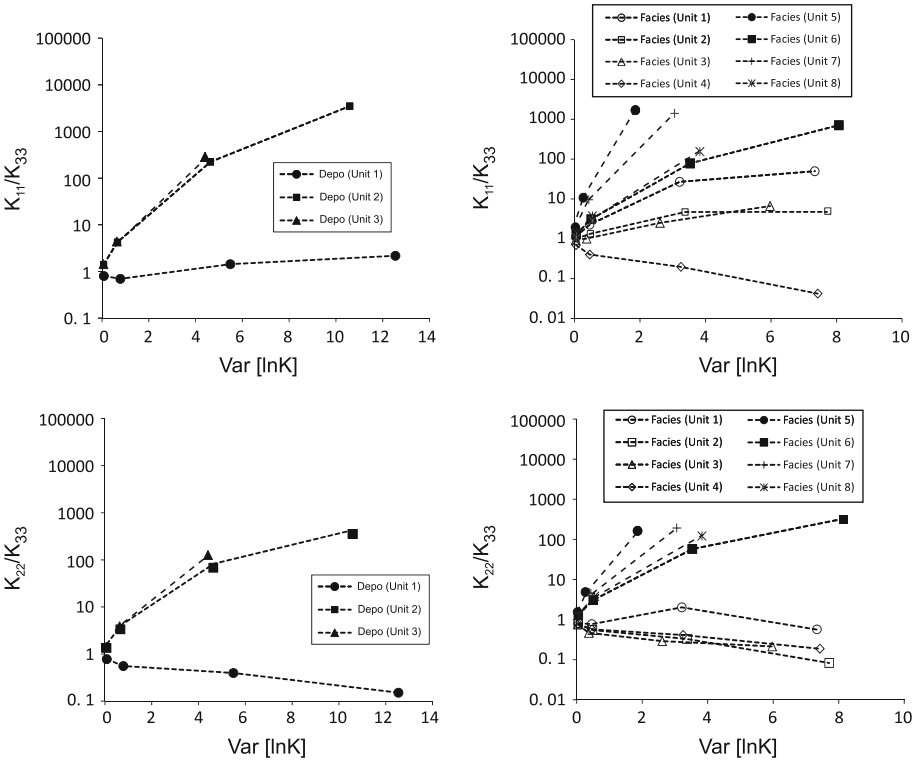

Fig. 3 Anisotropy ratio of the upscaled conductivity (K_{11}/K_{33}, K_{22}/K_{33}) versus ln$K$ variance for units of the Depositional and Facies Models

In Eclipse, to ensure that each external aquifer maintains a constant potential during simulation, a large water volume (4.6×10^{20} stb) is assigned to the aquifers (Schlumberger 2009). In running the simulations, a model run is considered to have reached steady state when: (1) pressure at each grid cell is constant over time; (2) inflow rate (from the external aquifer of higher potential into the model) is equal to the outflow rate (from the model into the external aquifer of lower potential); (3) computed potential gradient is stable and reaches the same value as the specified one. Since Eclipse employs iterative solvers, an initial pressure field must be provided. How close this initial field is to the final solution is found to have a significant impact on the length of time it takes for the simulation to reach steady-state. To provide best-guess initial pressure, a test run is first conducted in the heterogeneous model. The resulting steady-state pressure data are exported to provide the initial pressure for all simulations (due to homogenization, the steady-state pressure fields of all models are similar). Using this approach, all models reached steady-state fairly rapidly.[3]

To assess the accuracy of the HSMs, two prediction metrics are used: fluid potential and flow rate through the outflow boundary. Since at steady state, mass balance is well maintained

[3] Eclipse 300 runs simulations in either a blackoil mode or a compositional mode. To understand the impact of different modes on the computed single-phase flow rate and fluid potential, steady-state simulation results for the x directional flow are obtained using both modes. For all models, at all variances (up to 7.0), difference between these modes in terms of their computed flow rate and average field pressure is negligibly small. In the following analysis, all runs are conducted with the compositional mode.

(e.g., difference between inflow and outflow rates is typically less than 0.01 stb/day), only the outflow rate is used. In the following subsections, each prediction metric is presented. Impact of variance on the accuracy of the HSMs is discussed. Diagonal tensor approximation is also discussed.

3.2.1 Fluid Potential

Using results from all models, an absolute potential deviation (APD) can be computed for each grid cell of the HSM: APD=$|\Phi_{\text{HSM}} - \Phi_{\text{ref}}|$, Φ_{ref} is prediction by the heterogeneous (or reference) model. For each HSM, APD on the top surface of the grid is shown, one for each flow direction (x-flow, y-flow, and z-flow) (Fig. 4; $\sigma_f^2 = 1.0$). For each HSM (one column), the pattern of APD is distinctly different from one another when flow direction varies. When flow occurs in the same direction (one row), all HSMs display similar APD patterns. APD is then checked layer by layer. Again, similar patterns persist among the HSMs whenever the boundary condition is the same. At this variance level, spatial distribution of APD appears sensitive to the boundary condition, but not to the homogenization level. Same result is observed for the low and high variance cases (not shown). However, in the high variance case, though the APD pattern remains insensitive with the homogenization level, along any flow direction, magnitude of APD increases significantly with variance. Clearly, variance level is important to the *accuracy* of flow prediction.

When flow is lateral (x or y), APD map of a given HSM changes only slightly in the vertical direction. The map at the top surface closely resembles those at the other layers. At a given layer, APD is observed to be relatively small near the inflow and outflow boundaries, but becomes larger in the central areas (Fig. 4). Thus, when flow is parallel to stratification, higher accuracy in fluid potential prediction appears to be associated with the two sides where fluid potentials are fixed. The same result is observed when the system is at the lower and higher variance levels, i.e., the same APD pattern persisting in the vertical direction and higher accuracy near inflow/outflow boundaries. Clearly, variance has little influence on the pattern of APD.

When flow is vertical (perpendicular to stratification), the APD pattern on the top surface reflects the heterogeneity pattern at this location. For example, a lateral (along-x) APD zone exists, corresponding to the location of a high-K channel (Fig. 1). The APD also varies significantly in the vertical direction, i.e., the surface feature no longer persists with depth. After layer-by-layer inspection, the APD pattern now reflects the geologic structure at the layer depth. This result is also observed when the system is at lower and higher variances. Thus, when flow is perpendicular to stratification, APD pattern is dominated by geological structure while variance impacts the accuracy (as discussed above).

To compare the accuracy of fluid potential prediction among experiments (i.e., different boundary conditions), a global mean error (ME) in fluid potential is calculated:

$$\text{ME} = \frac{1}{n}\sum_{i=1}^{n} |\Phi_{\text{HSM}} - \Phi_{\text{ref}}| = \frac{1}{n}\sum_{i=1}^{n} \text{APD} \tag{10}$$

where n is the number of grid cells. ME is normalized by the absolute potential drop across the model in each experiment to compute a dimensionless mean relative error (MRE). MRE is an unbiased indicator of the relative deviation in predicting fluid potential (Zhang et al. 2006). For a given HSM, MRE can be used to compare among experiments. Results suggest that for each HSM, MRE in predicting the fluid potential is consistently the largest when the flow is along the y direction (Fig. 5).

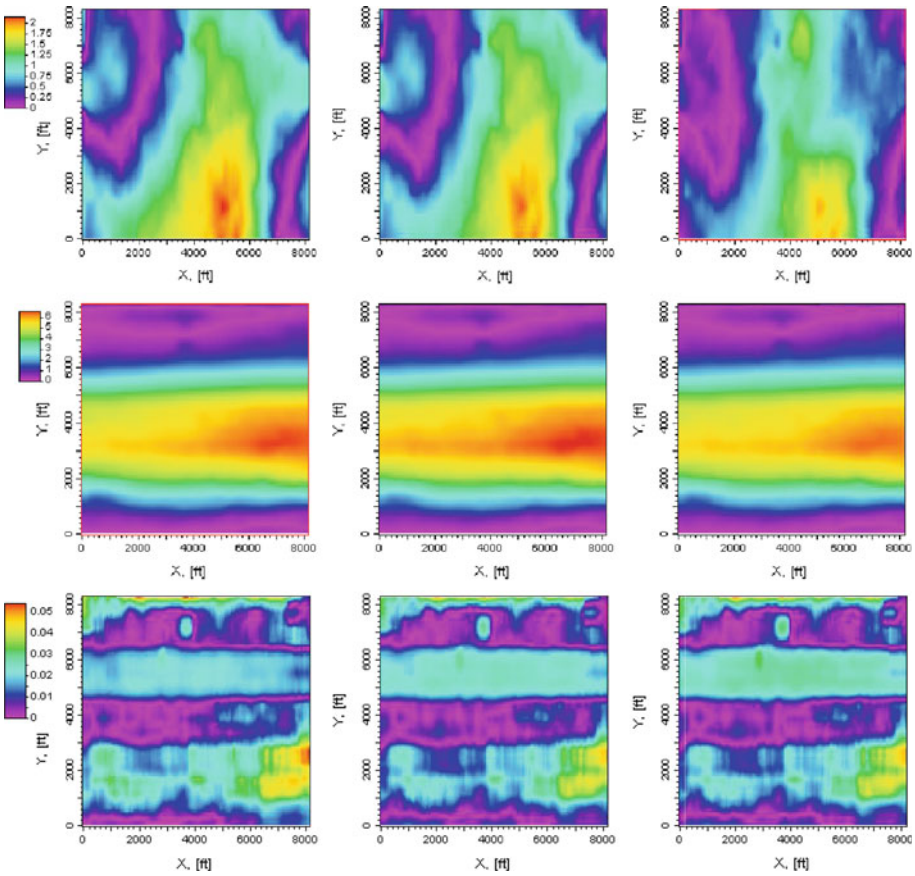

Fig. 4 Absolute potential deviation visualized at the top model layer for each HSM (system ln$K$ variance is 1.0). From top to bottom: x-flow, y-flow, and z-flow, respectively; from left to right: 1-Unit, 3-Unit, and 8-Unit, respectively

For a given HSM, when the magnitude of MRE is examined against variance, MRE increases with variance, for all flow directions (Fig. 5). At the variance of 0.1, MRE of all models ranges from 0.18% to 2.70%; at 1.0, 0.78% to 8.60%; at 7.0, 3.9% to 14.0%. This suggests that regardless of the type of the upscaled model used, fluid potential prediction becomes less accurate when variance increases. Further, no single HSM appears to be consistently the most accurate, when all flow directions and all variances are considered. For example, for x-flow, the 8-unit model is always the most accurate; for y-flow, no model is consistently the most accurate; for z-flow, the 1-unit model is the most accurate. In summary, boundary condition, heterogeneity variance, and homogenization level all impact the accuracy of the HSMs in predicting fluid potential.

3.2.2 Flow Rate

Table 4 presents the outflow rate computed by all models, for a variance up to 7.0. Figure 6 presents the flow rate prediction error by the HSMs. Results suggest: (1) along a given flow direction, prediction error in flow rate increases with variance, with one minor exception for

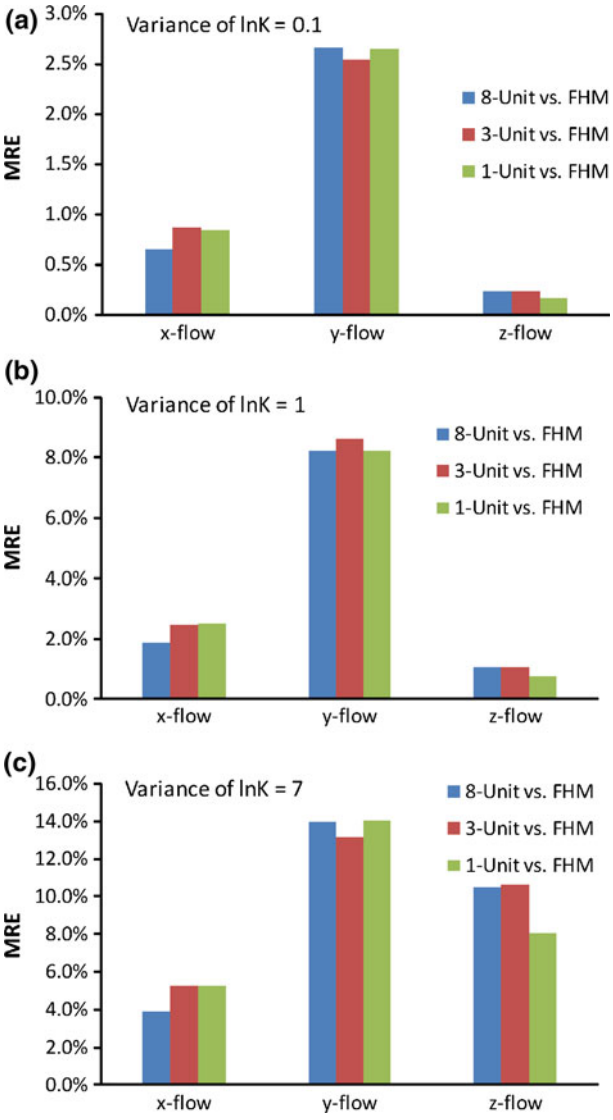

Fig. 5 Global MRE of the fluid potential predicted by the HSMs

y-flow (i.e., 3-unit model when $\sigma_f^2 = 1.0$). When $\sigma_f^2 \leq 1.0$, error in flow rate is around 1% or smaller. When $\sigma_f^2 = 7.0$, error ranges from 7.2% to 31.6% for x-flow, 5.6% to 11.1% for y-flow, and 6.9% to 20.6% for z-flow. (2) Along a given flow direction, error also increases with the level of homogenization (from the 8-unit to the 1-unit models), with the same minor exception as noted above. (3) At all variances, prediction accuracy is generally the highest for y-flow, then z-flow, and x-flow. This is opposite of that found for MRE in fluid potential prediction where y-flow yields the highest MRE. This discrepancy is not uncommon, however, as past work indicates that the accuracy in fluid potential prediction does not always correspond to the accuracy in flow rate prediction.

Table 4 Outflow rate predicted by all models. Based on results of the heterogeneous model ("Ref"), a relative error in flow rate prediction is computed for the HSMs

Variance of ln$K$	Models	x-flow		y-flow		z-flow	
		q (stb/day)	(Errror/ref) %	q (stb/day)	(Errror/ref) %	q (stb/day)	(Errror/ref) %
0.1	Ref	17.214	–	16.904	–	11.458	–
	8-Unit	17.214	0.000	16.888	−0.095	11.460	0.017
	3-Unit	17.231	0.099	16.885	−0.112	11.461	0.026
	1-Unit	17.240	0.151	16.898	−0.035	11.465	0.061
1	Ref	24.249		20.736		11.314	
	8-Unit	24.352	0.425	20.758	0.106	11.357	0.380
	3-Unit	24.678	1.769	20.735	−0.005	11.362	0.424
	1-Unit	24.792	2.239	20.871	0.651	11.425	0.981
7	Ref	94.442		57.227		9.480	
	8-Unit	101.258	7.217	60.410	5.562	10.134	6.899
	3-Unit	117.752	24.682	60.229	5.246	10.192	7.511
	1-Unit	124.329	31.646	63.604	11.143	11.431	20.580

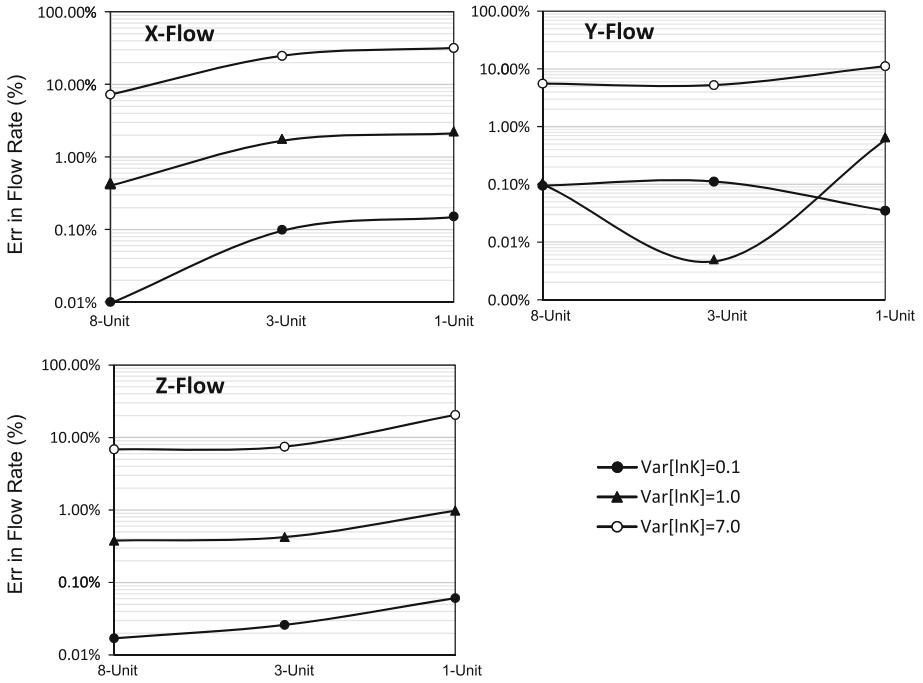

Fig. 6 Error in flow rate prediction by the HSMs. |Err| of Table 4 is plotted

Performance of the HSMs and the associated accuracy of the upscaled $\mathbf{K}^*$ could be improved if the model sub-domains are alternatively defined. This, however, does not mean that more subdivisions are necessarily the better. Under certain conditions (e.g., x-flow) (Fig. 6), division of the 3-unit model into eight units significantly enhances the accuracy in flow rate

prediction; under other conditions (e.g., z-flow), subdivision does not enhance this accuracy. Still under other conditions (noted above for y-flow at low variance), non-linear effects may occur.

For the models investigated here, which homogenization level is optimal for fluid potential or flow rate prediction depends on boundary condition and variance. In this study, the mapping used to define the sub-domains is based on kriging which can only provide descriptions of smoothed contacts, and sharp changes in material properties cannot be captured well. This limitation may have contributed to some aspects of the errors. Future work will consider using alternative approaches (e.g., percolation or connectivity analysis) to define the upscaling domains.

3.2.3 Diagonal Approximation

For efficiency, many flow simulators approximate conductivity full tensor with diagonal tensor. Frequently, full tensor information is either difficult to obtain, or if such information is available, it is more convenient to rotate the model coordinate axes to be aligned with the dominant K anisotropy axes. This approach, however, will not work well when different model sub-regions have different anisotropy directions. For the HSMs, errors in fluid potential and flow rate predictions are assessed when diagonal tensors (listed in Table 2) are used. Single-phase verification tests are again conducted, with flow along the x direction (results for y-flow and z-flow are expected to be similar).[4] For the models of this study, diagonal tensor approximation appears to give sufficiently accurate results in predicting both fluid potential and flow rate. This observation holds true at variance levels up to 7.0. Future work will assess other heterogeneities with significant dip angles.

3.3 Analytical Predictions

For the HSM units, principal components of the upscaled conductivity are compared to those predicted by analytical methods. Increasing variances are evaluated. Since theory by Gelhar (1993), as implemented in Eq. 7, is strictly valid for low variances, its predictions are made for $\sigma_f^2 = 0.1$ and 1.0 only. The high-variance version of Eq. 7 is also tested against the upscaling results and is found inaccurate at higher variances. For the four non-positive-definite cases, the horizontal components are compared to the analytical predictions.

Results suggest: (1) with a few exceptions, all analytical methods are nearly equally accurate in capturing the principal components when the variance is low, i.e., $\sigma_f^2 \leq 1.0$; (2) in estimating K_{11} and K_{22}, formulations proposed by Desbarats (1992) (Eq. 5) and Noetinger and Haas (1996) (Eq. 6) are consistently the most accurate at all variances;[5] (3) most analytical methods fail to capture K_{33} when variance is high. This suggests that estimation of the conductivity anisotropy ratio using analytical methods could be problematic. However, for those few cases that analytical methods do capture K_{33}, formulations of Desbarats (1992) and Noetinger and Haas (1996) are again the most accurate.

Analytical expressions of Desbarats (1992) and Noetinger and Haas (1996) are developed for multiGaussian media at low variances. Herein, their accuracy is also demonstrated on non-multiGaussian media while a full range of variance is tested. Since both formulations

[4] To understand the impact of different simulator modules, diagonal-tensor simulations are conducted with Eclipse 300 compositional mode, Eclipse 300 blackoil mode, and Eclipse 100. Different modules give consistent results.

[5] Results based on Eq. 6 vary from those of Eq. 5 by less than 1%. These two formulations are considered identical for the range of conductivity tested here.

are based on power averaging, this suggests that power law may be a reliable tool for predicting conductivities of irregular deposits. However, models of this study have univariate and bivariate characteristics that closely match the requirements of the analytical methods. The density function of $\ln K$ is unimodal, while the upscaling domains are large compared to the $\ln K$ integral scales (Table 1), satisfying theory requirement of an ergodic field for upscaling. Future work will evaluate the upscaling characteristics of deposits with multimodal densities as well as those that do not satisfy ergodicity.

4 Summary and Conclusion

Based on a synthetic aquifer exhibiting non-stationary, statistically anisotropic conductivity correlation, three HSMs are created: a Full Aquifer Model with a single unit, a Depositional Model with 3 units, and a Facies Model with 8 units. These models are hierarchical, reflecting a non-unique division of space and different heterogeneity homogenization levels. A geostatistical analysis of $\ln K$ is first conducted for the HSM units. Univariate and bivariate parameters such as mean and variance of $\ln K$ and directional integral scales are estimated. For these units, K is upscaled using numerical and analytical methods, for increasing $\ln K$ variances. Impact of variance on the accuracy of the upscaled conductivity and associated performance of the HSMs is assessed. Results are summarized as follows:

(1) the numerical method is capable of upscaling irregular domains with reasonable accuracy for a variance up to 7.0. For the models investigated, equivalent conductivity principal components at different scales are related by weighted arithmetic means. Given the existence of geometric connectivity, increasing variance can result in flow channeling in the lateral direction and increasing lateral:vertical anisotropy ratios of the equivalent conductivities.

(2) Accuracy of the upscaled conductivity and associated performance of the HSMs are sensitive to homogenization level, $\ln K$ variance, and boundary condition. At a fixed homogenization level and boundary condition, variance strongly influences the accuracy of the HSMs in predicting fluid potential and flow rate. The HSMs are more accurate when variance is low.
In fluid potential prediction, spatial pattern of the prediction error is sensitive to boundary condition, but insensitive to homogenization level and variance (magnitude of such error is sensitive to variance). In flow rate prediction, besides variance, performance of the HSMs is affected by boundary condition. Under some conditions, the 3-unit model appears optimal; under other conditions, the 8-unit model provides the optimal accuracy.

(3) At variance up to 7.0, HSM simulations conducted with full-tensor $\mathbf{K}^*$ versus diagonalized forms reveal little difference in flow rate and fluid potential predictions. For the heterogeneity evaluated here, diagonal tensor appears a good approximation.

(4) When the variance is low (less than 1.0), all analytical methods are found to be nearly equally accurate. However, when variance becomes higher, analytical methods generally become less accurate.
The current study conducts stratigraphic mapping to identify a set of hierarchical deposits. Hydrostratigraphic models of increasing complexity are then created. Units of these models, most are of irregular shape, are subjected to an upscaling analysis. Since a single grid is used by all models, numerical discretization error due to grid coarsening is not introduced into the upscaled models. The upscaled conductivity can thus be compared across scales. These models will be used in a future optimization analysis to understand

the effect of model complexity on prediction uncertainty. Though grid coarsening is not evaluated, this topic will be pursued in future work.

Acknowledgment Funding for this study was provided by a NSF grant EAR-0838250 awarded to the first author. We acknowledge the insightful comments of the anonymous reviewers.

References

Ababou, R.: Identification of effective conductivity tensor in randomly heterogeneous and stratified aquifers. In: Proceedings of the 5th Canadian/American Conference on Hydrogeology: Parameter Idenfitication and Estimation for Aquifer and Reservoir Characterization, pp. 155–157 (1991)

Ababou, R.: Random porous media flow on large 3-D grids: numerics, performance and application to homogenization. In: Wheeler, M.F. (ed.) Mathematics and its Applications: Environmental Studies—Math, Comput and Statistical Analysis, IMA vol 79, Chapter 1, pp. 1–25. Springer, New York (1996)

Desbarats, A.J.: Spatial averaging of hydraulic conductivity in three-dimensional heterogeneous porous media. Math. Geol. **24**(3), 249–267 (1992)

Desbarats, A.J., Srivastava, R.M.: Geostatistical analysis of groundwater flow parameters in a simulated aquifer. Water Resour. Res. **27**(5), 687–698 (1991)

Deutsch, C.V.: Geostatistical Reservoir Modeling. pp. 376 Oxford University Press, NY, USA (2002)

Durlofsky, L.J.: Upscaling and gridding of fine scale geological models for flow simulation. In: Proceedings of the 8th International Forum on Reservoir Simulation. Stresa, Italy, 20–25 June 2005

Gelhar, L.W.: Stochastic Subsurface Hydrology. Prentice Hall, Englewood Cliffs, NJ, USA (1993)

Gelhar, L.W., Axness, C.L.: Three-dimensional stochastic analysis of macrodispersion in aquifers. Water Resour. Res. **19**(1), 161–180 (1983)

Journel, A.G., Deutsch, C., Desbarats, A.J.: Power averaging for block effective permeability. SPE Paper 15128 (1986)

Knudby, C., Carrera, J.: On the relationship between indicators of geostatistical, flow and transport connectivity. Adv. Water Resour. **28**(4), 405–421 (2005)

Knudby, C., Carrera, J.: On the use of apparent hydrauilc diffusivity as an indicator of connectivity. J. Hydrol. **329**(3–4), 377–389 (2006)

Milliken, W., Levy, M., Strebelle, S., Zhang, Y.: The effect of geologic parameters and uncertainties on subsurface flow: deepwater depositional systems. SPE Paper 109950 (2007)

Noetinger, B., Haas, A.: Permeability averaging for well tests in 3D stochastic reservoir models. SPE J. **36653**, 919–925 (1996)

Renard, P., de Marsily, G.: Calculating equivalent permeability: a review. Adv. Water Resour. **20**(5-6), 253–278 (1997)

Ritzi, R.W., Allen-King, R.M.: Why did Sudicky (1986) find an exponential-like spatial correlation structure for hydraulic conductivity at the Borden research site? Water Resour. Res. (2007). doi:10.1029/2006WR004935

Sanchez-Vila, X., Girardi, J.P., Carrera, J.: A synthesis of approaches to upscaling of hydraulic conductivities. Water Resour. Res **31**(4), 867–882 (1995)

Sanchez-Vila, X., Carrera, J., Girardi, J.P.: Scale effects in transimissivity. J. Hydrol. **183**(1-2), 1–22 (1996)

Sanchez-Vila, X., Guadagnini, A., Carrera, J.: Representative hydraulic conductivities in saturated groundwater flow. Rev. Geophys. (2006). doi:10.1029/2005RG000169

Schlumberger: ECLIPSE, Technical Description 2009.2. Schlumberger (2009)

Wen, X.-H., Gómez-Hernández, J.: Upscaling hydraulic conductivities in heterogeneous media: an overview. J. Hydrol. (1996). doi:10.1016/S0022-1694(96)80030-8

Wen, X.H., Durlofsky, L.J., Edwards, M.G.: Use of border regions for improved permeability upscaling. Math. Geol. **35**(5), 521–547 (2003)

Zhang, D.: Stochastic methods for flow in porous media, coping with uncertainties. Academic Press, San Diego, CA (2002)

Zhang, Y.: Hierarchical geostatistical analysis of an experimental stratigraphy. Math. Geosci. (2008). doi:10.1007/s11004-008-9180-6

Zhang, Y., Gable, C.W., Person, M.: Equivalent hydraulic conductivity of an experimental stratigraphy—implications for basin-scale flow simulations. Water Resour. Res. (2006). doi:10.1029/2005WR004720

Zhang, Y., Gable, C. W., Sheets, B.: Equivalent hydraulic conductivity of three-dimensional heterogeneous porous media: an upscaling study based on an experimental stratigraphy. J. Hydrol. **388**, 304–320 (2010). doi:10.1016/j.jhydrol.2010.05.009